

Two-photocurrent devices

Matteo G. A. Paris

Arbeitsgruppe 'Nichtklassische Strahlung' der Max-Planck-Gesellschaft

Rudower Chaussee 5, 12489 Berlin, Germany

PARIS@PHOTON.FTA-BERLIN.DE

Abstract. Heterodyne, eight-port homodyne and six-port homodyne detectors belong to the class of two-photocurrent devices. Their full equivalence in probing radiation field has been proved both for ideal and not fully efficient photodetectors. The output probability distribution has been also evaluated for a generic probe mode.

1. Introduction

In order to gain information about a quantum state of the radiation field one has to measure some observable. The measurement process unavoidably involves some kind of interaction, thus coupling the mode under examination to one or more other modes of the field. One has to admit that, in general, the measured observable is not defined on the sole Hilbert space of the signal mode [1]. On the contrary, it reflects properties of the global state, possibly entangled, coming from the interaction among the signal mode and the set of the probe modes. Sometimes, it is possible to get rid of these probe modes, so that the statistics of the output is related only to the quantum statistics of the signal mode. This, as an example, is the case of balanced homodyne detectors [2]. In that case, in fact, an appropriate rescaling of the output photocurrent allows to completely neglect the local oscillator in the definition of the measured observable, which simply results to be proportional to the signal field quadrature $\hat{a}(\phi) = \frac{1}{2}(a^\dagger e^{i\phi} + a e^{-i\phi})$.

However, in more general cases this procedure cannot be pursued and the output statistics always remind us the way we are probing the signal under examination. This is a common feature of three relevant detection schemes in quantum optics, which provide different setup for jointly measuring a couple of photocurrents. They are the heterodyne [3, 4, 5], the eight-port homodyne [6, 7, 8, 9] and the recently introduced six-port homodyne detectors [10, 11].

It is a purpose of this paper to show that, although they involve very different ways of coupling signal to probe modes, they provide the same information on the signal under examination. Actually, we will prove their full equivalence by demonstrating that their

output photocurrents have the same operatorial form. More surprisingly, this remains true also when taking into account the inefficiency of photodetection, even though the latter occurs at very different stages in the three detection schemes.

The paper will be organized as follows. In the next section we briefly review how to describe inefficient photodetection in terms of beam splitters and ideal detectors. In the three sections 3,4 and 5 we will examine the three detection schemes respectively, in order to show that all of them jointly measure the real and the imaginary part of the complex photocurrent [4, 12]

$$\hat{Z} = a + b^\dagger, \quad (1)$$

being a the signal mode and b a probe mode. The inefficiency of realistic photodetectors will be also taken into account, in order to show it does not affect the equivalence of the considered detection schemes.

In section refs:pom we will derive the output statistics of considered schemes as members of the more general class of two-photocurrent devices. Section 7 will close the paper with some concluding remarks.

2. Inefficient photodetection

The final stage of any detection scheme is represented by photodetection, namely counting photon through their conversion to electric pulses. Let us consider a light beam $\hat{\rho}$ entering a phototube which converts to electric pulses a fraction ζ of the incoming photons. By keeping open the detector window for a time interval T , the probability $P_m(T)$ of counting m photons is given by [13]

$$P_m(T) = \text{Tr} \left\{ \hat{\rho} : \frac{[\zeta \hat{I}(T)T]^m}{m!} \exp[-\zeta \hat{I}(T)T] : \right\}, \quad (2)$$

where $: : \text{denotes normal ordering of operator and } \hat{I}(T) \text{ is the beam intensity}$

$$\hat{I}(T) = \frac{2\epsilon_0 c}{T} \int_0^T \hat{\mathbf{E}}^{(-)}(\mathbf{r}, t) \cdot \hat{\mathbf{E}}^{(+)}(\mathbf{r}, t) dt. \quad (3)$$

$\hat{\mathbf{E}}^{(\pm)}$ denotes the positive (negative) frequency part of the field. For a single-mode field excited in a stationary state Eq. 2 can be rewritten as

$$P_m^n = \text{Tr} \left\{ \hat{\rho} \frac{(\eta a^\dagger a)^m}{m!} \exp(-\eta a^\dagger a) \right\}, \quad (4)$$

being $[a, a^\dagger] = 1$ the single mode field operator and $\eta = \zeta c \hbar \omega / V$ the global quantum efficiency of the photodetectors. For unit quantum efficiency this coincides with the actual photon number distribution of the state under examination

$$P_m^1 = \rho_{mm} \equiv \langle m | \hat{\rho} | m \rangle, \quad (5)$$

whereas, in the realistic case of non-unit quantum efficiency Eq. (4) becomes a binomial convolution [14]. In formula

$$P_m^\eta = \sum_{n=m}^{\infty} \rho_{nn} \binom{n}{m} \eta^m (1-\eta)^{n-m}. \quad (6)$$

Let us now consider the scheme in Fig. 1. The signal mode a is impinged in a beam splitter of transmissivity τ whose second port b is placed in the vacuum. A perfect ($\eta = 1$) photodetection on the exiting mode reveals m photons with a probability

$$P_m = \text{Tr} \left(\hat{U}_\tau (\hat{\rho} \otimes |0\rangle\langle 0|) \hat{U}_\tau^\dagger |m\rangle\langle m| \otimes \hat{1} \right), \quad (7)$$

being $\hat{1}$ the identity operator on the second input of the beam splitter and

$$\hat{U}_\tau = \exp \left\{ i \arctan \sqrt{\frac{1-\tau}{\tau}} (a^\dagger b - ab^\dagger) \right\},$$

the evolution operator of the beam splitter. A straightforward calculation shows that

$$P_m = \sum_{n=m}^{\infty} \rho_{nn} \binom{n}{m} (1-\tau)^{n-m} \tau^m. \quad (8)$$

Eq. (8) coincides with Eq. (6) for $\tau = \eta$. This means that a photodetection process with efficiency η is equivalent to a perfect photodetection process performed on the original signal mixed with vacuum by a beam splitter with a value of the transmissivity equal to the quantum efficiency [15, 16]. In the following we will adopt this equivalent scheme.

3. Eight-port homodyne detector

Eight-port homodyne detector is known for a long time for the joint determination of phase and amplitude of the field in the microwave domain. It was introduced in the optical domain by Walker and Carrol [6] and successively analyzed by different authors [7, 8, 9, 17, 18, 19, 20, 21, 22, 23, 24, 25, 26, 27]. A schematic diagram of the experimental setup is reported in Fig. 2. There are four balanced beam splitters whereas a $\pi/2$ phase shifter is inserted in one arm. The four input modes are denoted by a_k , $k = 1, \dots, 4$ whereas the detected output modes are denoted by b_k , $k = 1, \dots, 4$. There are four identical photodetectors whose quantum efficiency is given by η . The *noise* modes used to take into account inefficiency, according to the scheme of the previous section, are denoted by u_i , $i = 1, \dots, 4$. We consider a_1 as the signal mode, whereas a_2 is referred to be the idler of the device. The mode a_3 is unexcited, whereas a_4 is placed in a highly excited coherent state $|z\rangle$ provided by an intense laser beam (local oscillator). The detected photocurrents are $\hat{I}_k = b_k^\dagger b_k$, $k = 1, \dots, 4$ which form the eight-port homodyne

observables

$$\begin{aligned}\hat{\mathcal{Z}}_1 &= \frac{\hat{I}_2 - \hat{I}_1}{2\eta|z|} \\ \hat{\mathcal{Z}}_2 &= \frac{\hat{I}_4 - \hat{I}_3}{2\eta|z|}.\end{aligned}\tag{9}$$

The latter are derived by rescaling the difference photocurrent, each of them obtained in an homodyne scheme. For this reason eight-port homodyne is known also as double-homodyne detection. In Eq. (9) η denotes the quantum efficiency of the photodetectors whereas $|z|$ is the intensity of the local oscillator. In order to obtain $\hat{\mathcal{Z}}_1$ and $\hat{\mathcal{Z}}_2$ in terms of the input modes we first note that the input-output mode transformation is necessarily linear, as only passive components are involved in the detection scheme [28, 29]. Thus, we can write

$$b_k = \sum_{l=1}^4 M_{kl} a_l,\tag{10}$$

where the transformation matrix can be computed starting from the corresponding transformations for the beam splitters and the phase shifter [32]

$$\mathbf{M} = \frac{1}{\sqrt{4}} \begin{bmatrix} 1 & 1 & 1 & 1 \\ 1 & i & -1 & -i \\ 1 & -1 & i & -1 \\ 1 & -i & -1 & i \end{bmatrix}.\tag{11}$$

Eqs. (10) and (11) together with the equivalent scheme for the inefficient detector leads to the following expression for the output modes

$$\begin{aligned}b_1 &= \sqrt{\eta} [a_1 + a_2 + a_3 + a_4] + \sqrt{1-\eta} u_1 \\ b_2 &= \sqrt{\eta} [a_1 + ia_2 - a_3 - ia_4] + \sqrt{1-\eta} u_2 \\ b_3 &= \sqrt{\eta} [a_1 - a_2 + ia_3 - a_4] + \sqrt{1-\eta} u_3 \\ b_4 &= \sqrt{\eta} [a_1 - ia_2 - a_3 + ia_4] + \sqrt{1-\eta} u_4.\end{aligned}\tag{12}$$

Upon inserting Eqs. (12) in Eq. (9) and considering the limit of highly excited local oscillator we obtain the eight-port photocurrents in terms of the input modes

$$\begin{aligned}\hat{\mathcal{Z}}_1 &= \hat{a}_1(0) + \hat{a}_2(0) + \sqrt{\frac{1-\eta}{\eta}} [\hat{u}_1(0) - \hat{u}_2(0)] + O\left[\frac{1}{|z|}\right] \\ \hat{\mathcal{Z}}_2 &= -\hat{a}_1(\pi/2) + \hat{a}_2(\pi/2) + \sqrt{\frac{1-\eta}{\eta}} [\hat{u}_3(\pi/2) - \hat{u}_4(\pi/2)] + O\left[\frac{1}{|z|}\right].\end{aligned}\tag{13}$$

In Eq. (13) $\hat{a}(\phi)$ denotes a quadrature of the field. The complex photocurrent $\mathcal{Z} = \mathcal{Z}_1 + i\mathcal{Z}_2$ is given by

$$\mathcal{Z} = a_1 + a_2^\dagger,\tag{14}$$

for unit quantum efficiency, whereas for non unit quantum efficiency it becomes a Gaussian convolution of Eq. (14), we will consider this point in detail in 6.

It is worth noticing here that the mode transformation defined by Eqs. (10) and (11) is distinctive for a canonical 4×4 -port linear coupler as defined in Refs. [30, 31]. It has been rigorously shown [32] that a $N \times N$ -port linear coupler can always be realized in terms of a number of beam splitters and phase-shifters. However, this implementation is, in general, not unique. The interest of eight-port homodyne scheme lies in the fact it provides the minimal scheme for realizing a 4×4 -multiport [33]. If one considers the multiport as a given *black-box* device the eight-port homodyne scheme can be depicted as in Fig. 3. This will facilitate the comparison with the six-port homodyne detection presented in Section 5.

4. Heterodyne detector

Heterodyne detection scheme is known for a long time in radiophysics. It has been introduced in the domain of optics [3, 4, 5, 34] in order to describe the joint measurement of two conjugated quadratures of the field. The term 'heterodyne' is used as the involved field modes are excited on different frequencies.

In Fig. 4 we show a schematic diagram of the detector. We denote by $\hat{\mathbf{E}}_S$ the signal field, whereas $\hat{\mathbf{E}}_{LO}$ describes the local oscillator. The field $\hat{\mathbf{E}}_L$ accounts for the losses due to inefficient photodetection. The input signal is excited in a single mode (say a) at the frequency ω , whereas also the local oscillator is excited in only one mode at the frequency ω_0 . This local oscillator mode is placed in a strong coherent state $|z\rangle$ by means of an intense laser beam. The beam splitter has a transmissivity given by τ , whereas the photodetectors shows quantum efficiency η . The heterodyne output photocurrents are given by the real $\hat{\mathcal{Z}}_1$ and the imaginary $\hat{\mathcal{Z}}_2$ part of the complex photocurrent $\hat{\mathcal{Z}}$. The latter is obtained after the rescaling of the output photocurrent \hat{I} , which is measured at the intermediate frequency $\omega_I = \omega - \omega_0$. By Fourier transform of Eq. (3) we have

$$\hat{I}(\omega_I) = \int_{\mathbf{R}} d\omega' \hat{\mathbf{E}}_O^{(-)}(\omega' + \omega_I) \hat{\mathbf{E}}_O^{(+)}(\omega'), \quad (15)$$

being $\hat{\mathbf{E}}_O^{(\pm)}$ positive and negative part of the output field. In terms of the input fields Eq. (15) can be written as

$$\hat{I}(\omega_I) = \int_{\mathbf{R}} d\omega' \left[\sqrt{\eta\tau} \hat{\mathbf{E}}_S^{(-)}(\omega' + \omega_I) + \sqrt{\eta(1-\tau)} \hat{\mathbf{E}}_{LO}^{(-)}(\omega' + \omega_I) + \sqrt{1-\eta} \hat{\mathbf{E}}_L^{(-)}(\omega' + \omega_I) \right] \\ \left[\sqrt{\eta\tau} \hat{\mathbf{E}}_S^{(+)}(\omega') + \sqrt{\eta(1-\tau)} \hat{\mathbf{E}}_{LO}^{(+)}(\omega') + \sqrt{1-\eta} \hat{\mathbf{E}}_L^{(+)}(\omega') \right]. \quad (16)$$

Heterodyne photocurrent is obtained by the following rescaling

$$\hat{\mathcal{Z}} = \lim_{\tau \rightarrow 1, |z| \rightarrow \infty} \frac{\hat{I}(\omega_I)}{|z| \eta \sqrt{\tau(1-\tau)}} \quad \text{with } |z| \sqrt{1-\tau} \text{ constant.} \quad (17)$$

Physically this definition corresponds to require a very intense local oscillator, which however is allowed only for a little mixing with the signal mode [35]. In this limit only terms containing the local oscillator field $\mathbf{E}_{LO}^{(\pm)}(\omega_0)$ at the frequency ω_0 can survive in Eq. (16), so that we have

$$\hat{\mathcal{Z}} = \hat{\mathcal{Z}}_1 + i\hat{\mathcal{Z}}_2, \quad (18)$$

where

$$\begin{aligned} \hat{\mathcal{Z}}_1 &= \hat{a}(0) + \hat{c}(0) + \sqrt{\frac{1-\eta}{\eta}} (\hat{u}_1(0) - \hat{u}_2(0)) \\ \hat{\mathcal{Z}}_2 &= -\hat{a}(\pi/2) + \hat{c}(\pi/2) + \sqrt{\frac{1-\eta}{\eta}} (\hat{u}_1(\pi/2) - \hat{u}_2(\pi/2)). \end{aligned} \quad (19)$$

In writing Eq. (19) we have substituted

$$\begin{aligned} c &\leftarrow \hat{\mathbf{E}}_S^{(+)}(2\omega_0 - \omega) \\ u_1 &\leftarrow \hat{\mathbf{E}}_L^{(+)}(\omega) \quad , \\ u_2 &\leftarrow \hat{\mathbf{E}}_L^{(+)}(2\omega_0 - \omega) \end{aligned} \quad (20)$$

for the relevant modes involved. Provided u_1 and u_2 to be noise modes placed in the vacuum the expression (19) for the heterodyne photocurrents leads to the identical output statistics of eight-port homodyne photocurrents, the mode c playing the role of the idler of the device. The full equivalence of the two detection schemes has been thus proved.

5. Six-port homodyne detector

A linear, symmetric three-port optical coupler is a straightforward generalization of the customary lossless symmetric beam splitter. The three input modes a_i , $i = 1, 2, 3$ are combined to form 3 output modes b_j , $j = 1, 2, 3$. In analogy to lossless beam splitters, which are described by unitary 2×2 matrices [36], any lossless triple coupler is characterized by a unitary 3×3 matrix [37, 38]. For the symmetric case we have the form

$$\mathbf{T} = \frac{1}{\sqrt{3}} \begin{pmatrix} 1 & 1 & 1 \\ 1 & \exp\{i\frac{2\pi}{3}\} & \exp\{-i\frac{2\pi}{3}\} \\ 1 & \exp\{-i\frac{2\pi}{3}\} & \exp\{i\frac{2\pi}{3}\} \end{pmatrix}, \quad (21)$$

where each matrix element T_{ij} represents the transmission amplitude from the i -th input port to the j -th output port, that is $b_j = \sum_{k=1}^3 T_{jk} a_k$.

Such devices have already been implemented in single-mode optical fiber technology and commercial triple coupler have been available for some time [39]. Any triple coupler can be also implemented by discrete optical components using symmetric beam splitters and phase shifters only [37]. As it has already mentioned in Section 3, this is due to remarkable mathematical fact that that any unitary M -dimensional matrix can be factorized into a sequence of 2-dimensional transformations plus phase-shift [32]. Moreover, this decomposition is not, in general, unique. In Fig. 5 a possible implementation of a triple coupler is schematically reported. Experimental realizations of triple couplers has been reported for both cases, the passive elements case and the optical fiber one [37, 38, 40, 41].

Let us now consider the measurement scheme of Fig. 6. The three input modes are mixed by a triple coupler and the resulting output modes are subsequently detected by three identical photodetectors. The measured photocurrents are proportional to \hat{I}_n , $n = 1, 2, 3$ given by

$$\hat{I}_n = b_n^\dagger b_n = \frac{1}{3} \sum_{k,l=1}^3 \exp \{i\theta_n(l-k)\} a_k^\dagger a_l, \quad \theta_n = \frac{2\pi}{3}(n-1). \quad (22)$$

After photodetection a Fourier transform (FT) on the photocurrents is performed

$$\hat{\mathcal{I}}_s \equiv \text{FT}(\hat{I}_1, \hat{I}_2, \hat{I}_3) = \frac{1}{\sqrt{3}} \sum_{n=1}^3 \hat{I}_n \exp \{-i\theta_n(s-1)\}, \quad s = 1, 2, 3. \quad (23)$$

This procedure is a straightforward generalization of the customary two-mode balanced homodyning technique. In that case, in fact, the sum and the difference of the two output photocurrents are considered, which actually represent the Fourier transform in a two-dimensional space. By means of the identity

$$\delta_3(s-1) = \frac{1}{3} \sum_{n=1}^3 \exp \left\{ i \frac{2\pi}{3} n(s-1) \right\}, \quad (24)$$

for the periodic (modulus 3) Kronecker delta δ_3 , we obtain our final expressions for the Fourier transformed photocurrents

$$\hat{\mathcal{I}}_1 = \frac{1}{\sqrt{3}} \{ a_1^\dagger a_1 + a_2^\dagger a_2 + a_3^\dagger a_3 \}, \quad (25)$$

$$\hat{\mathcal{I}}_2 = \frac{1}{\sqrt{3}} \{ a_1^\dagger a_2 + a_2^\dagger a_3 + a_3^\dagger a_1 \}, \quad (26)$$

$$\hat{\mathcal{I}}_3 = \frac{1}{\sqrt{3}} \{ a_1^\dagger a_3 + a_2^\dagger a_1 + a_3^\dagger a_2 \}. \quad (27)$$

$\hat{\mathcal{I}}_1$ gives no relevant information as it is insensitive to the phase of the signal field, whereas $\hat{\mathcal{I}}_2$ and $\hat{\mathcal{I}}_3$ are hermitian conjugates of each other and contain the relevant information in their real and imaginary part. In the following let us assume a_1 is the signal mode

and a_2 is fed by a highly excited coherent state $|z\rangle$ representing the local oscillator. For large $|z|$ the output photocurrents are intense enough to be easily detected. They can be combined to give the reduced photocurrents

$$\begin{aligned}\hat{\mathcal{Z}}_1 &= \sqrt{3} \frac{\hat{\mathcal{I}}_2 + \hat{\mathcal{I}}_3}{2|z|} = \hat{a}_1(0) + \hat{a}_3(0) + O\left[\frac{1}{|z|}\right] \\ \hat{\mathcal{Z}}_2 &= \sqrt{3} \frac{\hat{\mathcal{I}}_2 - \hat{\mathcal{I}}_3}{2i|z|} = -\hat{a}_1(\pi/2) + \hat{a}_3(\pi/2) + O\left[\frac{1}{|z|}\right],\end{aligned}\quad (28)$$

which we refer to as the *triple homodyne photocurrents*. Again the complex photocurrent $\hat{\mathcal{Z}} = \hat{\mathcal{Z}}_1 + i\hat{\mathcal{Z}}_2$ has the form $\hat{\mathcal{Z}} = a_1 + a_3^\dagger$, being a_1 the signal mode and a_3 the idler of the device.

When accounting for the non unit quantum efficiency η of the photodetectors the output modes are written as

$$b_j = \sqrt{\eta} \left(\sum_{k=1}^3 T_{jk} a_k \right) + \sqrt{1-\eta} u_j \quad j = 1, 2, 3,$$

so that the reduced photocurrents are now given by

$$\begin{aligned}\hat{\mathcal{Z}}_1 &= \sqrt{3} \frac{\hat{\mathcal{I}}_2 + \hat{\mathcal{I}}_3}{2\eta|z|} = \hat{a}_1(0) + \hat{a}_3(0) + \sqrt{\frac{1-\eta}{\eta}} [\hat{u}_1(0) - \hat{u}_3(0)] + O\left[\frac{1}{|z|}\right] \\ \hat{\mathcal{Z}}_2 &= \sqrt{3} \frac{\hat{\mathcal{I}}_2 - \hat{\mathcal{I}}_3}{2i\eta|z|} = -\hat{a}_1(\pi/2) + \hat{a}_3(\pi/2) + \sqrt{\frac{1-\eta}{\eta}} [\hat{u}_1(\pi/2) - \hat{u}_3(\pi/2)] + O\left[\frac{1}{|z|}\right].\end{aligned}\quad (29)$$

When, as it is the case, the modes u_j are placed in the vacuum the six-port photocurrents in Eq. (29) leads to the same statistics of the eight-port photocurrents in Eq. (13). Indeed, they describe different devices leading to the same amount of information on the signal mode a_1 . Some comments are, however, in order. By comparison of Fig. 3 and Fig. 6 it appears obvious that six-port homodyne is an optimized scheme relative to the eight-port one. One mode less is needed to reach the same amount of information, thus decreasing the possible sources of noise. The reason for this lies in the final stage of the two schemes. The Fourier transform of the six-port photocurrents, in fact, is a more effective procedure relative to the double-homodyne final stage of the eight-port scheme. This is related to the noise suppression mechanism of homodyne detection. The latter, in fact, is generalized to the multi-mode case by the Fourier transform rather than duplication of the original two-mode scheme.

6. Output statistics from a two-photocurrent device

In this section we analyze with some detail the output statistics of an abstract two-photocurrent device. The latter is characterized by the joint measurement of the real

$\widehat{\mathcal{Z}}_1$ and the imaginary $\widehat{\mathcal{Z}}_2$ part of the complex photocurrent

$$\widehat{\mathcal{Z}} = a + b^\dagger, \quad (30)$$

when equipped with perfect photodetectors. On the other hand, in the realistic case of inefficient photodetection the photocurrent is given by

$$\widehat{\mathcal{Z}} = a + b^\dagger + \sqrt{\frac{1-\eta}{\eta}} (u_1 + u_2^\dagger). \quad (31)$$

In Eqs. (30) and (31) a and b denote single mode radiation field which can be excited in any quantum state. The operators u_1 and u_2 also denote single mode radiation field, however strictly placed in the vacuum states. They are used to simulate losses due inefficient photodetection, according to the equivalent detection scheme of Section 2. In the following we will refer to the mode a as the signal mode which is under examination, whereas the mode b is in a known and fixed state, playing the role of the probe mode of the device. This is only for sake of convenience. It is obvious that the roles of the two modes can be interchanged and any argument can be reversed considering the mode b as a signal mode. According to this scheme we denote the outcome probability density distribution by $K_b(\alpha, \bar{\alpha})$. The latter describes, in the complex plane, the state of the mode a as probed by the mode b . Indeed, different choices for the probe mode lead to very different features in the probability distribution.

Each experimental random outcome (z_1, z_2) from the joint measurement of $\widehat{\mathcal{Z}}_1$ and $\widehat{\mathcal{Z}}_2$ can be considered as a point z in the complex plane. On the other hand, the output photocurrent $\widehat{\mathcal{Z}}$ is expressed as a sum of different contributions coming from different modes. Therefore, it appears intuitively rather obvious that the resulting probability distribution will be given by a convolution. To be more specific let us start by considering the ideal case of unit quantum efficiency $\eta = 1$. We write the probability distribution $K_b(\alpha, \bar{\alpha})$ as the Fourier transform

$$K_b(\alpha, \bar{\alpha}) = \int_{\mathbf{C}} \frac{d^2\gamma}{\pi^2} e^{\bar{\gamma}\alpha - \gamma\bar{\alpha}} \Xi(\gamma, \bar{\gamma}), \quad (32)$$

of the characteristic function

$$\Xi(\gamma, \bar{\gamma}) = \text{Tr} \left\{ \hat{\rho} \exp \left[\bar{\gamma} \widehat{\mathcal{Z}} - \gamma \widehat{\mathcal{Z}}^\dagger \right] \right\}, \quad (33)$$

being $\hat{\rho}$ the global density matrix describing both modes a and b . We consider probe mode to be independent on the signal mode, so that the input mode is factorized as

$$\hat{\rho} = \hat{\rho}_a \otimes \hat{\rho}_b. \quad (34)$$

Upon substituting Eqs. (30) and (34) in Eq. (33) we are able to write the characteristic function $\Xi(\gamma, \bar{\gamma})$ as a product

$$\Xi(\gamma, \bar{\gamma}) = \text{Tr} \left\{ \hat{\rho}_a \otimes \hat{\rho}_b \hat{D}_a(\gamma) \otimes \hat{D}_b(-\gamma) \right\} = \chi_a(\gamma, \bar{\gamma}) \chi_b(-\gamma, -\bar{\gamma}), \quad (35)$$

being

$$\hat{D}(\gamma) = \left\{ \hat{\rho} \exp \left[\gamma a^\dagger - \bar{\gamma} a \right] \right\}$$

the displacement operator and

$$\chi(\gamma, \bar{\gamma}) = \text{Tr} \left\{ \hat{\rho} \hat{D}(\gamma) \right\}$$

the single mode characteristics function, the latter entering in the definition of the Wigner function of a single mode radiation field [42, 43, 44]

$$W(\alpha, \bar{\alpha}) = \int \frac{d^2\lambda}{\pi} \chi(\lambda, \bar{\lambda}) \exp \left\{ \bar{\lambda} \alpha - \lambda \bar{\alpha} \right\} . \quad (36)$$

We now insert Eq. (35) in Eq. (32). By means of Eq. (36) and using the convolution theorem we arrive at the final result

$$K_b(\alpha, \bar{\alpha}) = W_a(\alpha, \bar{\alpha}) \star W_b(-\alpha, -\bar{\alpha}) = \int_{\mathbf{C}} \frac{d^2\beta}{\pi^2} W_b(\alpha + \beta, \bar{\alpha} + \bar{\beta}) W_a(\beta, \bar{\beta}) , \quad (37)$$

the symbol \star denoting convolution. Eq. (37) provides a justification for referring to the mode b as the probe of the device. In fact, it acts as a filter on the signal' Wigner function. The latter is not a genuine probability distribution, as it can be negative when describing quantum interference. Thus, it cannot be directly sampled by experiments. However, the convolution (37) make it more regular, leading to $K_b(\alpha, \bar{\alpha})$ which is a measurable distribution.

Phase space density as in Eq. (37) have been already introduced by Wodkiewicz [45, 46, 47] to account for the effect of the measuring apparatus in a joint measurement of conjugated variables. Originally, they have been termed phase-space *propensities*. More recently, they also have been used in entropic description of quantum mechanical states [48, 49]. Two-photocurrent devices appear as the natural setup to start from, in order to experimentally access such kind of phase-space distribution.

Wigner function, though it contains a complete description of the quantum state, cannot be directly measured. The phase distributions $K_b(\alpha, \bar{\alpha})$ are smoothed version of it, corresponding to the occurrence of additional noise of purely quantum origin. Indeed, two-photocurrent devices provide the generalized joint measurement of position and momentum, thus unavoidably introducing additional noise by first principles [34, 50, 51]. The crucial point to notice here is that they offer the remarkable possibility to manipulate this quantum noise. As it emerges from Eq. (37) it can be redirected in the desired region of the complex plane by suitable choice of the probe mode, according to the kind of information of which is of interest.

In order to incorporate the effects of inefficient detection we first note that Eq. (31) differs from Eq. (30) by two additional *additive* terms. Therefore, further convolutions to the original Wigner function are expected. Indeed, the characteristic function of the

whole device is now expressed as

$$\begin{aligned} \Xi_\eta(\gamma, \bar{\gamma}) &= \chi_a(\gamma, \bar{\gamma}) \chi_b(-\gamma, -\bar{\gamma}) \times \\ &\times \chi_{u_1} \left(\sqrt{\frac{1-\eta}{\eta}} \gamma, \sqrt{\frac{1-\eta}{\eta}} \bar{\gamma} \right) \chi_{u_2} \left(-\sqrt{\frac{1-\eta}{\eta}} \gamma, -\sqrt{\frac{1-\eta}{\eta}} \bar{\gamma} \right) \end{aligned} \quad (38)$$

where characteristic function for the noise modes can be easily evaluated as

$$\chi_{u_j} \left(-\sqrt{\frac{1-\eta}{\eta}} \gamma, -\sqrt{\frac{1-\eta}{\eta}} \bar{\gamma} \right) = \exp \left[-\frac{1-\eta}{2\eta} |\gamma|^2 \right] \quad j = 1, 2. \quad (39)$$

Upon inserting Eqs. (38) and (39) in Eq. (32) we obtain our final result, namely the output probability distribution $K_{b\eta}(\alpha, \bar{\alpha})$ of a two-photocurrent device equipped with photodetectors of quantum efficiency η

$$K_{b\eta}(\alpha, \bar{\alpha}) = K_{b1}(\alpha, \bar{\alpha}) \star G_\eta(\alpha, \bar{\alpha}) = \int_{\mathbf{C}} \frac{d^2\beta}{\pi^2} K_b(\beta, \bar{\beta}) \exp \left[-\frac{\eta}{1-\eta} |\alpha - \beta|^2 \right], \quad (40)$$

being $K_{b1}(\alpha, \bar{\alpha})$ the probability distribution obtained for ideal photodetection and

$$G_\eta(\alpha, \bar{\alpha}) = \exp \left[-\frac{\eta}{1-\eta} |\alpha|^2 \right]$$

the filter function summarizing the effects of inefficient photodetection.

7. Conclusions

In this paper we have introduced the class of two-photocurrent devices. This kind of detectors are characterized by the fact that they jointly measure the real and the imaginary part of the complex photocurrent $\mathcal{Z} = a + b^\dagger$, where a and b describe two single mode of the radiation field. Eight-port homodyne, heterodyne and six-port homodyne detectors belong to this general class, thus their fully equivalence in probing radiation field has been proved. It has also been proved that this equivalence still holds when the inefficiency of the photodetection process is taken into account. This is an interesting and unexpected result, as photodetection takes place at very different stages in the three detection schemes.

The three schemes analyzed in this paper are equivalent from the point of view of provided information on the measured signal. Nevertheless, they have different physical implementations which have to be compared. We pointed out the advantages of the six-port homodyne scheme in comparison with the customary eight-port one. Actually, it provides the minimal scheme to access generalized phase space distribution [52].

In a two-photocurrent device a generalized joint measurement of position and momentum is performed on the signal mode. This results in a smoothing of the signal

Wigner function to a measurable distribution, which represents the output probability distribution of the measurement. Some additional noise is unavoidably introduced, according to the Heisenberg principle for joint measurement. However, the filtering process has been shown to be a convolution with the Wigner function of the probe mode. Therefore, it is possible to manipulate and redirect the noise. A suitable choice of the probe mode enhances different features of the signal' phase space distribution, according to the kind of desired information.

Acknowledgment

I would thank Prof. Harry Paul for his kind hospitality in the group 'Nichtklassische Strahlung' of Max-Planck society and Prof. Mauro D'Ariano for introducing me to the subject of phase-space measurements. I would also thank Valentina De Renzi, Ole Steuernagel, Gabriel Drobny, Alexei Chizhov and Alfred Wünsche for profitable discussions. This work has been partially supported by the University of Milan by a scholarship for postgraduate studies in foreign countries.

References

- [1] Busch P, Lahti P J 1995 *Riv. Nuovo Cim.* **18** 1
- [2] Yuen H P, Chan V W S 1983 *Opt. Lett.* **8** 177
- [3] Yuen H P, Shapiro J H 1980 *IEEE Trans. Inf. Theory* **IT-26** 78
- [4] Shapiro J H, Wagner S S 1984 *IEEE J. Quant. Electron.* **QE-20** 803
- [5] Shapiro J H 1985 *IEEE J. Quant. Electron.* **QE-21** 237
- [6] Walker N G, Carrol J E 1984 *Electron. Lett.* **20** 981
- [7] Walker N G, Carrol J E 1986 *Opt. Quant. Electron.* **18** 355
- [8] Walker N G 1987 *J. Mod. Opt.* **34** 15
- [9] Lai Y, Haus H A 1989 *Quantum Opt.* **1** 99
- [10] Paris M G A, Chizhov A, Steuernagel O 1996 *Opt. Comm.* **134** 117
- [11] Zucchetti A, Vogel W, Welsch D G 1996 *Phys. Rev.* **A54** 856
- [12] D'Ariano G M, Sacchi M F 1995 *Phys. Rev.* **A52** R4309
- [13] Kelley P L, Kleiner W H, 1964 *Phys. Rev.* **136** 316
- [14] Mandel L, Wolf E 1995 *Optical Coherence and Quantum Optics*, (Cambridge University Press)
- [15] Leonhardt U, Paul H 1993 *Phys. Rev.* **A48** 4598
- [16] D'Ariano G M, Macchiavello C, Paris M G A 1995 *Phys. Lett.* **A198** 286
- [17] Noh J W, Fougères A, Mandel L 1991 *Phys. Rev. Lett.* **67** 1426
- [18] Noh J W, Fougères A, Mandel L 1992 *Phys. Rev.* **A45** 424
- [19] Noh J W, Fougères A, Mandel L 1992 *Phys. Rev.* **A46** 2840
- [20] Bandilla A, Ritze H H 1993 *Quantum Opt.* **5** 213
- [21] Freyberger M, Schleich W P 1993 *Phys. Rev.* **A47** R30
- [22] Leonhardt U, Paul H 1993 *Phys. Rev.* **A47** 2460
- [23] D'Ariano G M, Paris M G A 1993 *Phys. Rev.* **A48** R4039
- [24] D'Ariano G M, Paris M G A 1994 *Phys. Rev.* **A49** 3022
- [25] Freyberger M, Heni M, Schleich W P 1995 *Quantum Opt.* **7** 187
- [26] Paris M G A 1996 *Phys. Rev.* **A53** 2658
- [27] Paris M G A 1996 *Opt. Comm.* **124** 277
- [28] Stenholm S 1994 *J. Mod. Opt.* **41** 2483
- [29] Stenholm S 1995 *Appl. Phys.* **B60** 243
- [30] Törmä P, Stenholm S, Jex I 1995 *Phys. Rev.* **A52** 4853
- [31] Jex I, Stenholm S, Zeilinger A 1995 *Opt. Comm.* **117** 95
- [32] Reck M, Zeilinger A, Bernstein H J, Bertani P 1994 *Phys. Rev. Lett.* **73** 58
- [33] Törmä P, Jex I, Stenholm S 1996 *J. Mod. Opt.* **43** 245
- [34] Yuen H P 1982 *Phys. Lett.* **A91** 101
- [35] Paris M G A 1996 *Phys. Lett.* **A217** 78
- [36] Campos R A, Saleh B E A, Teich M C 1989 *Phys. Rev.* **A40** 1371
- [37] Mattle K, Michler M, Weinfurter H, Zeilinger A, Zukowski M 1995 *Appl. Phys.* **B60** S111
- [38] Weihs G, Reck M, Weinfurter H, Zeilinger A 1996 *Opt. Lett.* **21** 302
- [39] Sheem S K 1981 *J. Appl. Phys.* **52** 3865
- [40] Hariharan P, Sen D 1959 *J. Sci. Instr.* **36** 70
- [41] Zernike F 1950 *J. Opt. Soc. Am.* **40** 326
- [42] Wigner E P 1932 *Phys. Rev.* **40** 749
- [43] Cahill K E, Glauber R J 1969 *Phys. Rev.* **177** 1857

- [44] Cahill K E, Glauber R J 1969 *Phys. Rev.* **177** 1882
- [45] Wodkiewicz K 1984 *Phys. Rev. Lett.* **52** 1064
- [46] Wodkiewicz K 1986 *Phys. Lett.* **A115** 304
- [47] Wodkiewicz K 1988 *Phys. Lett.* **A129** 1
- [48] Buzek V, Keitel C H, Knight P L 1995 *Phys. Rev.* **A51** 2575
- [49] Buzek V, Keitel C H, Knight P L 1995 *Phys. Rev.* **A51** 2594
- [50] She C Y, Heffner H 1966 *Phys. Rev.* **152** 1103
- [51] Arthurs E, Goodman M S 1988 *Phys. Rev. Lett.* **60** 2447
- [52] Paris M G A, Steuernagel O 1996, in preparation.

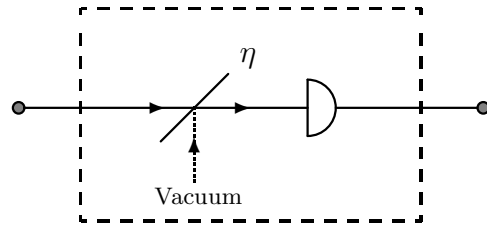


Figure 1. Equivalent scheme for inefficient photodetection.

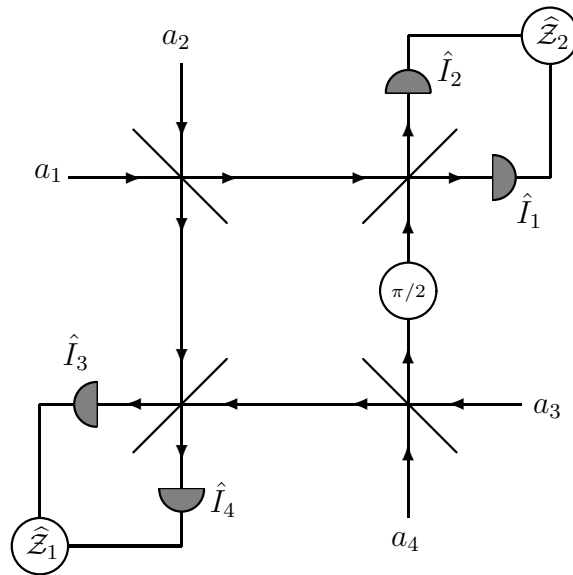


Figure 2. Schematic diagram of an eight-port homodyne detector.

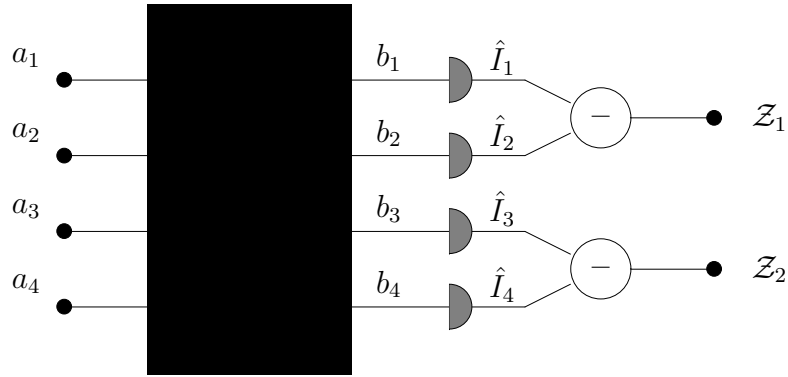


Figure 3. Eight-port homodyne detector as a multiport homodyne.

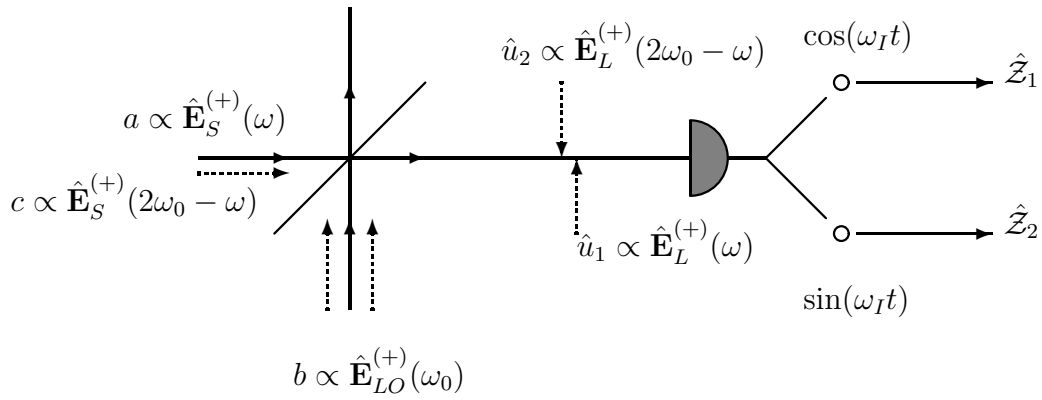


Figure 4. Schematic diagram of a heterodyne detection. Relevant modes are explicitly pointed out.

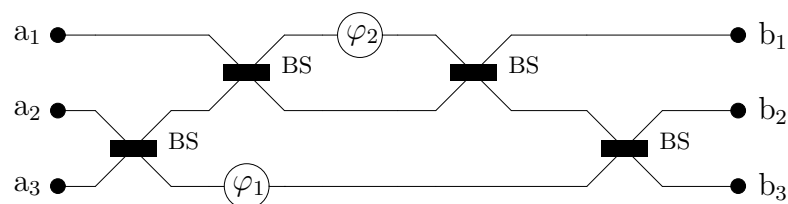


Figure 5. Realization of a triple coupler in terms of 50:50 beam splitters (BS) and phase shifters ' φ '. In order to obtain a symmetric coupler the following values has to be chosen: $\varphi_1 = \arccos(1/3)$ and $\varphi_2 = \varphi_1/2$.

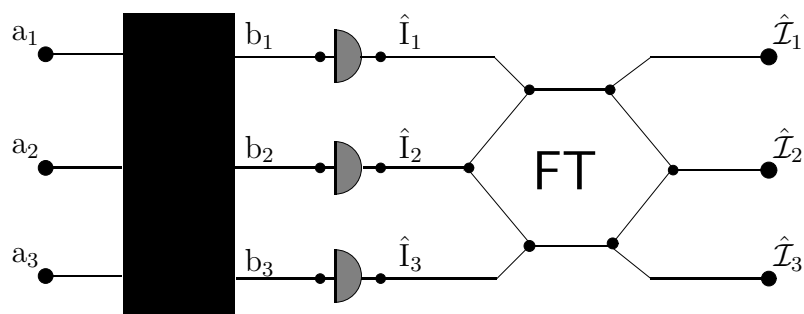


Figure 6. Outline of triple coupler homodyne detectors: The hexagonal box symbolizes the electronically performed Fourier transform (FT).